POLITECNICO DI TORINO

MASTER's Degree in MATERIALS ENGINEERING FOR INDUSTRY 4.0

MASTER's Degree Thesis

Thermochromic 3D-printed structures from biobased acrylated systems

Supervisors

Prof. Marco Sangermano

Candidate

Aiko Matsubar

FEBRUARY 2026

Index

1 Introduction

Since the Industrial Revolution, global warming has been driven by the increasing concentration of greenhouse gases in the atmosphere and has led to severe climate variations all over the world [1]. Atmospheric CO_2 level has dramatically risen, contributing to melting ice caps, sea-lever rise and changes in oceanic or atmospheric circulation patterns. Those changes have influenced the ecosystems, loss of biodiversity or habitat destruction. Of course, even human beings have been facing economic and social impacts, such as reduced agricultural productivity, rising risk of disasters, and anxiety of water or energy resources for future. Those issues became the trigger for us to reduce both our dependence on fossil fuels and greenhouse gas emissions. Sustainable technologies and alternative materials have been helping us to reach our goals.

In this context, bio-based polymers have attracted attention as natural alternatives to fossil-derived plastics, as they can contribute to reducing CO_2 emissions, and their utilization is being explored in various regions and fields. Those polymers offer advantages in biodegradability, recycling potential, and environmentally friendly since they are produced from renewable sources such as plant starch, cellulose, or vegetable oils, The development of new materials derived from bio-based polymers is expected to support the establishment of a sustainable society [2].

As interest in creating new materials continues to grow, material processing technologies have also advanced, with increasing demand for methods that minimize energy consumption and material waste. UV-induced polymer curing has become known as a sustainable technology because it suppresses the emission of volatile organic compounds (VOCs) and consumes less energy compared with heat-based processes, compared with conventional heat-base curing. Those benefits enable us to obtain products with precise control over polymerization kinetics and material properties.

This technology has also been applied to Additive Manufacturing (AM) technologies from the perspective of reducing energy requirements. Moreover, due to the AM capability of depositing material only where needed to build, the waste generation must be minimized and enabling the production of near-net-shape or net-shape products [3].

One of the most popular technologies of AM must be 3D printing. It enables layer-by-layer fabrication of objects directly from 3D computer models. By depositing materials only where needed, AM reduces resource consumption and increases material efficiency, thus it allows the creation of complex geometries

which were difficult or even impossible with traditional manufacturing techniques.

1.1 Overview of 3D printing technologies

AM is based on the concept of depositing materials only where needed according to a 3D computer model. This approach reduces material waste and enables the fabrication of highly complex structures, which are difficult to achieve with conventional manufacturing methods. The range of materials available for AM has expanded considerably, from conventional thermoplastics and thermosetting resins to even metals and ceramics, allowing for a broad spectrum of applications. AM is particularly well suited for mass customization, as customized products can be produced without extensive retooling even in large-scale manufacturing. Moreover, the open-source culture of the 3D printing community enables us to create a collaborative environment that promotes technological advancement.

According to the ASTM Standard F2792, 3D printing technologies are categorized into seven groups below [4,5]

1.1.1 Binder Jetting

Binder jetting uses two types of materials; a powdered material that becomes the final printed object, and a binder material (typically a liquid) that bonds the powder particles together. For building materials, not only metals and alloys but also ceramics can be used. In fact, any material that can be supplied in powder form is compatible. Moreover, the process can even support full-color printing. In binder jetting, a thin layer of powder is spread, and then binder is selectively jetted onto the required regions based on the CAD model. By repeating this process, the part is built layer by layer. Because the process does not involve heating during printing, no residual thermal stresses remain in the fabricated part, and support structures are unnecessary. Both of which are significant advantages of Binder Jetting process. On the other hand, since the material is typically consolidated through sintering, there is always a possibility that pores will remain, which can lead to reduced mechanical properties. The schematic of Binder Jetting are shown below in Figure 1.1 and 1.2 [6,7, 8].

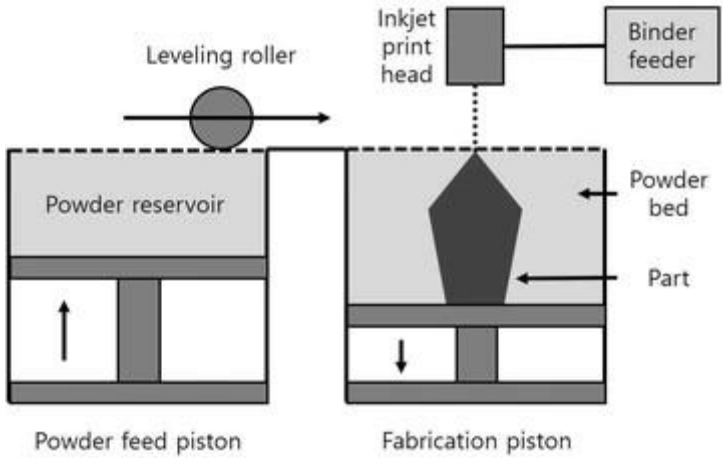

Figure 1.1 Schematic of Binder Jetting technique.

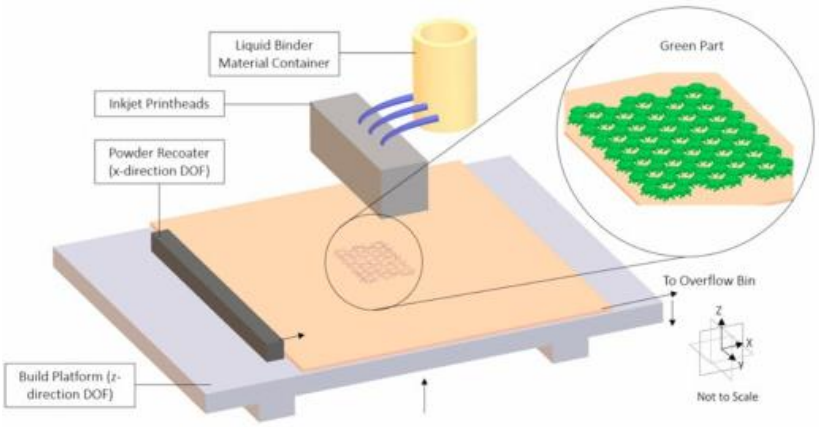

Figure 1.2 Schematic image of Binder Jetting technique.

1.1.2 Directed Energy Deposition (DED)

Directed Energy Deposition (DED) uses focused thermal energy, such as a laser, electron beam, or plasma arc, to melt material where it is deposited. It is often used for the repair of components and enables the fabrication of parts of higher quality. The feedstock can be in powder or wire form, which allows for flexible material choices. Advantages include high deposition rates and the ability to work with multiple alloys in a single build. On the other hand, there are some limitations including surface roughness, thermal

residual stress, and relatively simple geometries compared with powder bed techniques. Figure 1.3 shows the refiguration of DED process and laser deposition methods [9].

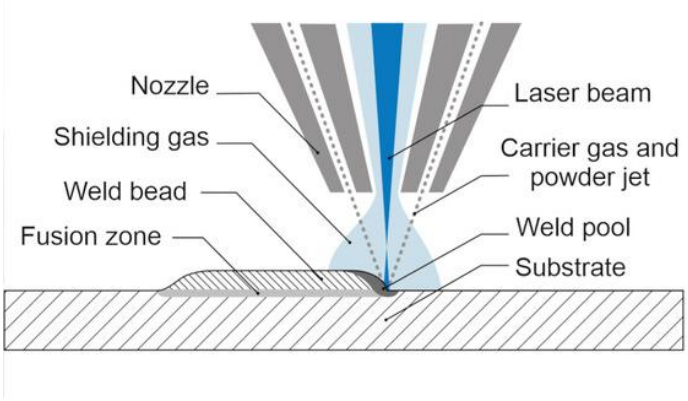

Figure 1.3 Schematic of DED process.

1.1.3 Material Extrusion

Material extrusion-based 3D printing technologies are widely used because they are low cost and capable of multi-material and multi-color fabrication. In this process, material is extruded through a nozzle and deposited layer by layer to build the part. Fused Deposition Modeling (FDM) (Figure 1.4) is an example of material extrusion, in which a thermoplastic filament is heated until it becomes semi-molten and then extruded as a thin bead that is deposited along a prescribed path . The filament is deposited layer by layer according to a 3D model. Materials commonly used include PLA, ABS, and composite filaments with fillers such as carbon fibers. The process relies on thermal softening and cooling-induced solidification, which involves physical bonding between layers. Advantages include low cost, accessibility, and suitability for prototyping. In contrast, limitations include anisotropic mechanical properties due to layer adhesion and relatively low resolution compared with photopolymerization-based methods [10].

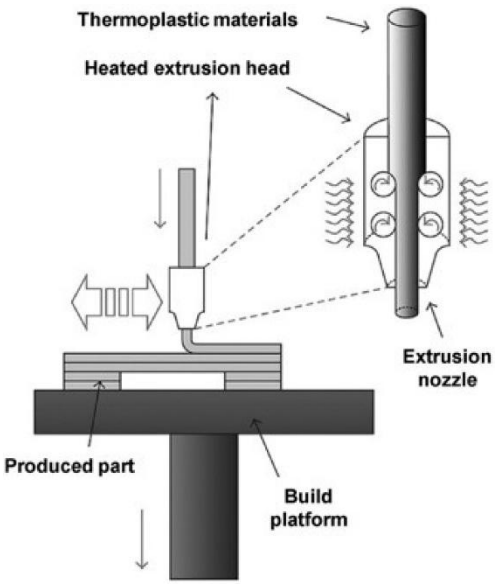

Figure 1.4 Schematic of FED.

1.1.4 Material Jetting

Material jetting is a technique in which the droplets of build material are selectively deposited, which are then cured by UV light. As shown in Figure 1.5, a print head ejects a photosensitive material, which is cured by UV irradiation to form each layer of the part. Multi-material deposition is possible, enabling the creation of parts with different mechanical or optical properties in a single build. For the limitations, it requires higher material cost and the need for support structures for overhangs. Resolution depends on droplet size, curing time, and resin properties. Though there are several limitations, Material jetting enables us to obtain high dimensional accuracy and good surface finishes [11].

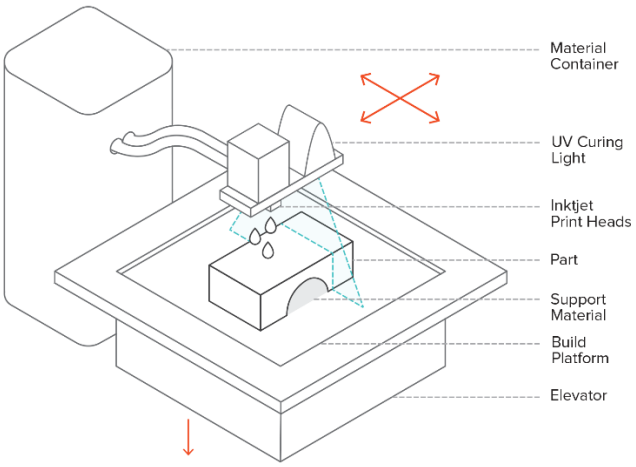

Figure 1.5 Schematic of Material Jetting.

1.1.5 Powder Bed Fusion

Powder bed fusion includes techniques such as Electron Beam Melting (EBM), Selective Laser Sintering (SLS), and Selective Heat Sintering (SHS). All of them use an electron beam or a laser to melt or fuse powder materials. SLS (Figure 1.6) enables high-speed and high-precision fabrication using metal, plastic, and ceramic powders. SHS melts thermoplastic powder using a thermal print head, while EBM uses an electron beam as the energy source to heat and melt metallic and ceramic materials [12].

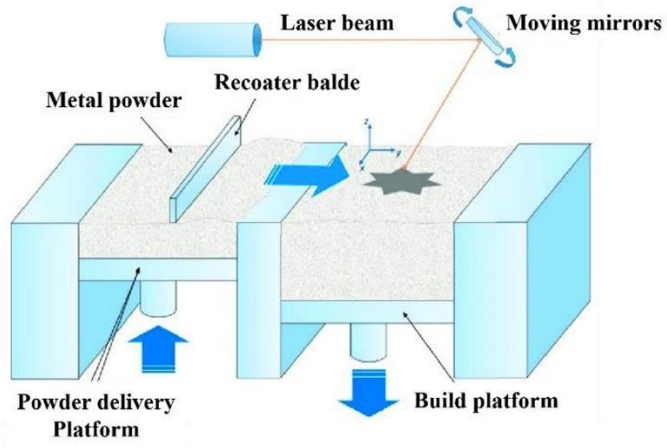

Figure 1.6 SLS system setup.

1.1.6 Sheet Lamination

Sheet lamination is a method in which material sheets are bonded together to create an object. A representative example is Laminated Object Manufacturing (LOM, Figure 1.7). Compared with other AM techniques, LOM is known for its low cost, short processing time, ability to produce relatively complex shapes, and ease of material handling. The method involves cutting sheets or roll materials layer by layer, then stacking and bonding them. Each layer is precisely cut using a cutter or a laser and subsequently bonded(Figure 1.8) [8, 13].

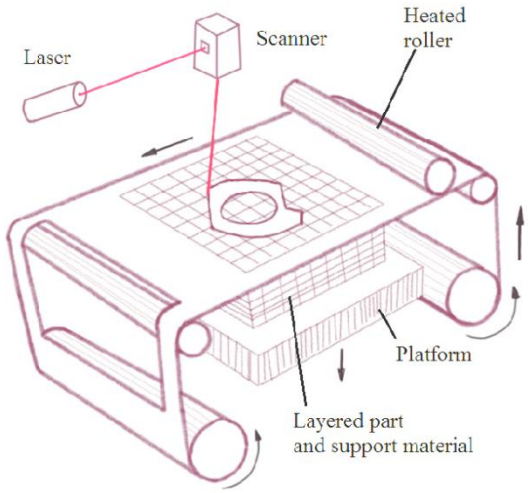

Figure 1.7 Schematic of LOM.

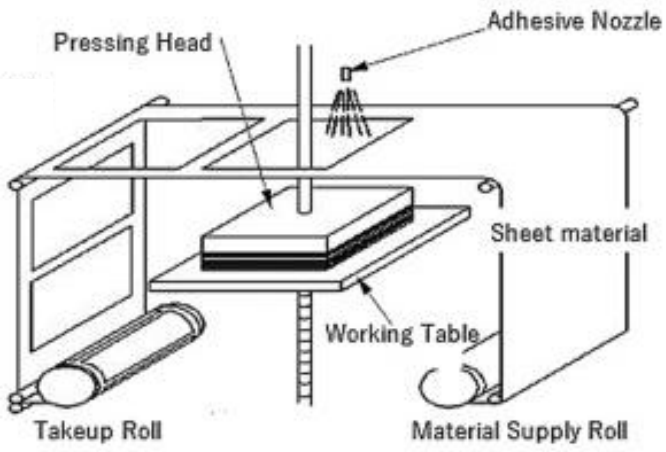

Figure 1.8 Schematic for laminated object manufacturing techniques.

1.1.7 Vat Photopolymerization

Vat Photopolymerization is a widely used 3D printing technique in which liquid photoreactive polymers are cured into solid forms using laser, visible, or UV light. By exposing light, photoinitiators in the vat are activated and initiate polymerization, during which monomers form long polymer chains. Techniques include Stereolithography (SLA), Digital Light Processing (DLP), and Continuous Liquid Interface Production (CLIP).

Curing involves a photopolymerization reaction, forming covalent bonds that solidify the resin layer by layer. Materials include acrylate-, methacrylate- and epoxy-based resins, often with functional additives such as dyes or particles. Process parameters such as light intensity, exposure time, or layer thickness significantly affect mechanical properties and surface finishing [15].

1.2 Vat Photopolymerization technologies

In this paragraph, some examples of Vat Photopolymerization are reported in detail.

As already mentioned in section 1.1.7, Vat Photopolymerization is an AM technique where a liquid photopolymer is cured into solid structures by exposing a light source. Streolithography (SLA) and Digital Light Processing (DLP) are the most commercialized ones of Vat photopolymerization. Recently, other methods have also been developed such as Continuous Liquid Interface Production (CLIP), Two-Photon Polymerization (2PP) and Computed Axial Lithography (CAL) [15].

1.2.1 Stereolithography (SLA)

Stereolithography (SLA, Figure 1.9) is a technique that selectively cures liquid photopolymer resin using a UV laser. The method is one of oldest techniques forms of Vat Photopolymerization and remains used for high precision applications widely.

In this process, the laser traces the pattern of each layer on the surface of the resin, and cures it

point by point. Once a layer is cured, the build platform moves vertically, exposing fresh resin for the next layer to be cured. SLA can produce parts with smooth surfaces and fine details, making it suitable for dental, jewelry, and microfluidic applications. Limitations include slower build speeds and the need for support structures for overhangs, as well as post-curing steps to achieve full mechanical strength

SLA systems come in two configurations: top-down and bottom-up. In the top-down configuration, the laser is positioned above the resin tank, and the platform descends into the resin (Figure 1.10). In contrast, in the bottom-up configuration, the light source is located beneath the resin tank and irradiates through a transparent bottom surface (Figure 1.11) [8, 14, 16].

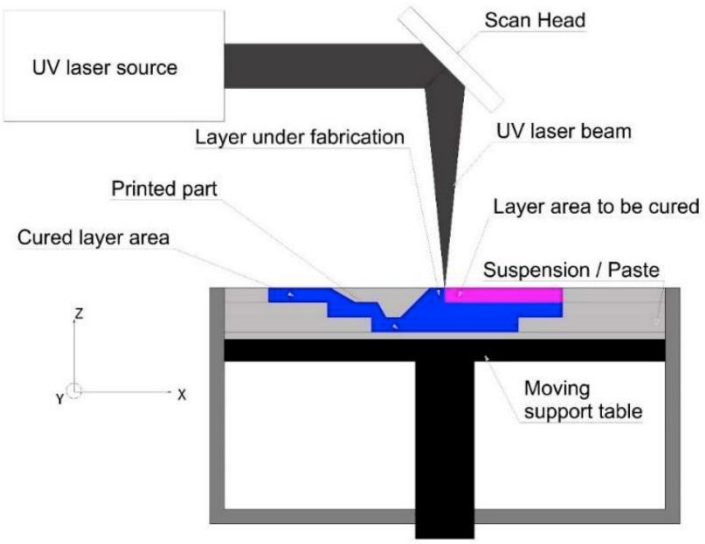

Figure 1.9 Representation of SLA technology.

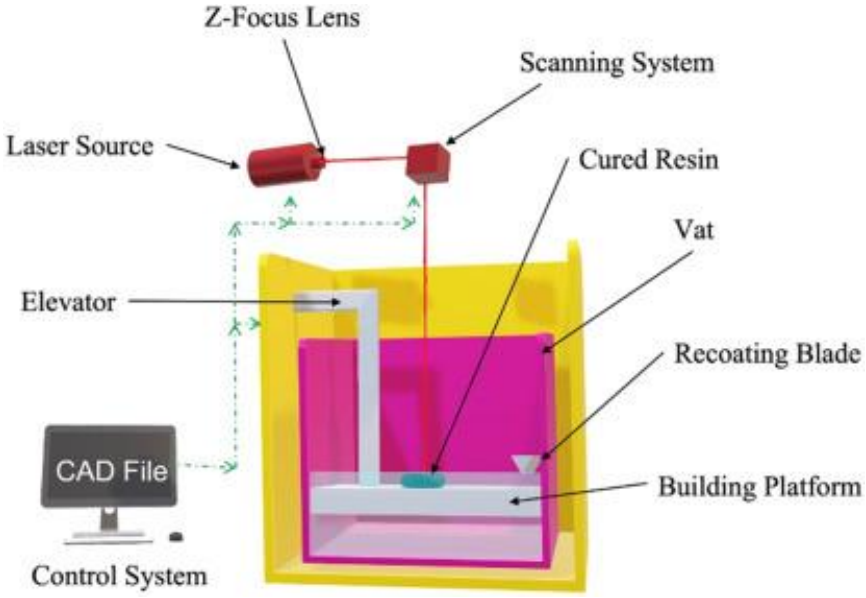

Figure 1.10 Top-Down configuration for SLA technology.

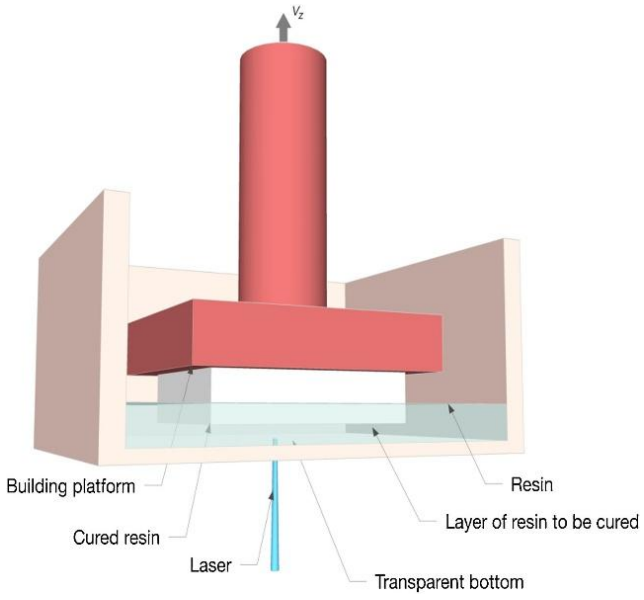

Figure 1.11 Bottom-Up setup for SLA technology.

1.2.2 Continuous Liquid Interface Production (CLIP)

Continuous Liquid Interface Production (CLIP) is an approach that advances conventional DLP technology by introducing a continuous printing process. In CLIP, digital projection using LEDs is employed, and the bottom of the resin vat is made of a transparent, oxygen-permeable material. This creates so called a “dead zone” in which a thin layer of resin remains uncured due to oxygen inhibition, allowing liquid resin to continuously flow between the cured part and the bottom surface of the vat. As a result, the build platform can rise continuously rather than in discrete layer-by-layer steps, enabling smoother surfaces and significantly faster printing (Figure 1.12) [17].

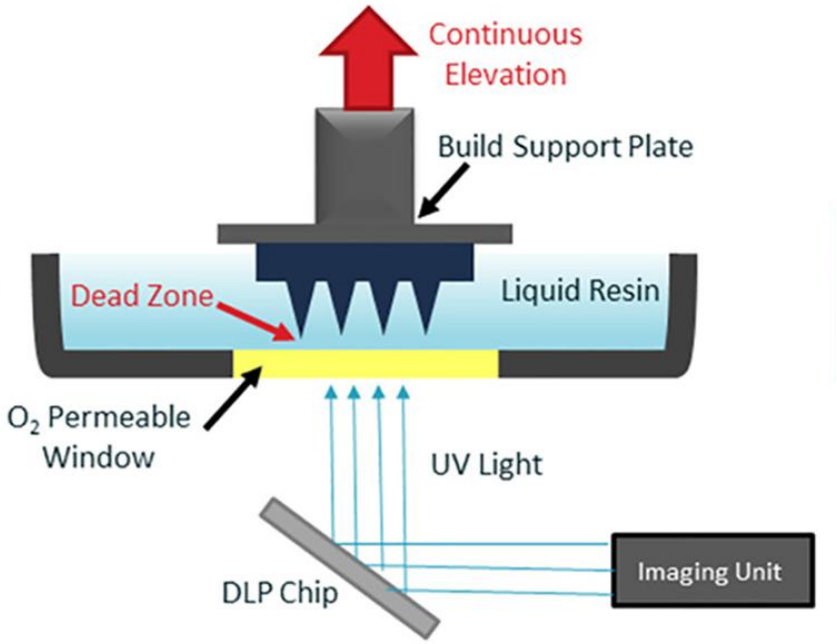

Figure 1.12 Representation of CLIP process technology.

1.2.3 Two-Photon Polymerization (2PP)

Two-Photon Polymerization (2PP) is an advanced technique which uses a femtosecond laser. When the laser irradiates the resin, two photons are absorbed almost simultaneously within a very

small volume inside the material, inducing a photopolymerization reaction (Figure 1.13). This enables the fabrication of extremely fine structures with a high resolution of approximately 100 nm. While the high precision of 2PP makes it ideal for producing complex microstructures, it is limited by the relatively small volume, which is typically restricted to about one cubic centimeter [18].

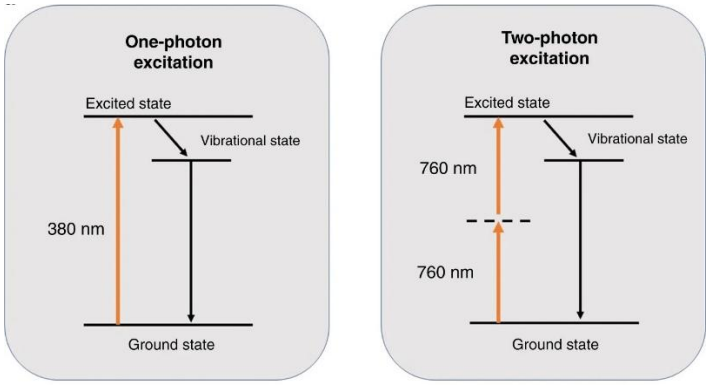

Fig 1.13 Comparison of the absorption of energy a single photon by UV light and two photons by near-infrared light.

1.2.4 Computed Axial Lithography (CAL)

Computed Axial Lithography (CAL) irradiates a rotating volume of photosensitive resin with a continuous sequence of 2D images from multiple directions. As these light patterns intersect, the resin cures all at once and continuously into the desired shape (Figure 1.14). This technique enables high-speed fabrication and produces smoother surfaces. However, its resolution is lower than that of other methods and is generally limited to the millimeter scale [19].

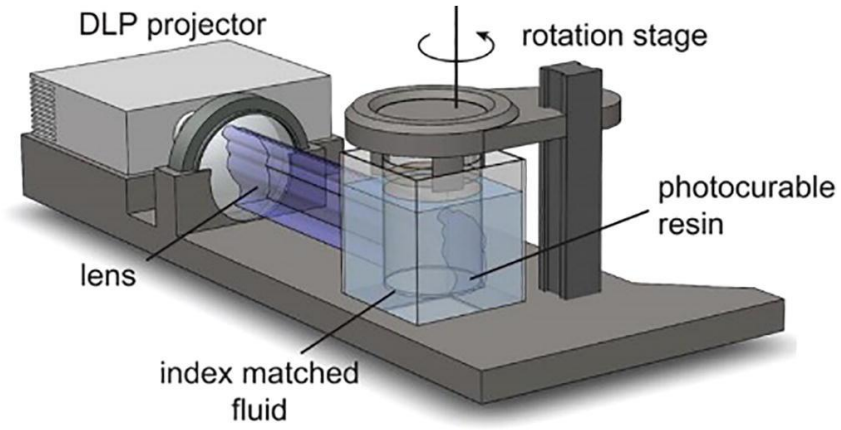

Figure 1.14 Schematic of CAL.

1.2.5 Digital Light Processing (DLP)

Digital Light Processing (DLP, Figure 1.15) is one of vat photopolymerization methods that uses a conventional light source and a liquid crystal display (LCD) panel to project and expose an entire resin layer simultaneously. By curing the entire layer at once through reflected light, high fabrication speed can be achieved. Key parameters include exposure time, wavelength, and light intensity. This method is suitable for producing high-resolution and high-quality parts. DLP employs a bottom-up configuration in which the light source is placed beneath the vat and reducing the influence of oxygen inhibition. The resolution of DLP is determined by the pixel matrix of the digital micromirror device (DMD) or LCD, and the projected image resolution directly affects the quality of the printed objects. Therefore, high-density pixel matrices enable fast fabrication with high resolution and precision, making DLP advantageous for applications requiring both speed and accuracy [14, 20].

Resins used in DLP must possess two key properties: photopolymerizability activated by photoinitiators and suitable flowability. Commonly used resins include acrylates, methacrylates, and epoxy resins, all of which can be efficiently cured by light. Resin viscosity is a critical parameter, as sufficiently low viscosity ensures uniform spreading within the vat and helps prevent defects. Low-viscosity resins also promote molecular diffusion, leading to more efficient photopolymerization and shorter processing times. In contrast, high-viscosity resins can cause non-uniform resin distribution, hinder the separation of the build platform in bottom-up systems, and negatively affect the final printing resolution. To adjust viscosity, diluents can be added, thereby broadening the range of

photopolymers applicable to DLP. In general, the appropriate viscosity range is approximately 0.2–10 Pa·s, and the shear rate during fabrication is around 5–20 s^{-1} [21].

Resins suitable for DLP typically undergo two types of photopolymerization reactions: radical and cationic polymerization. Among these, acrylate and methacrylate resins based on radical polymerization are the most widely used. In radical polymerization, photoinitiators absorb light and decompose to generate free radicals, which initiate polymer chain growth. Polyglycerol-based acrylate monomers commercially available as the SYntech SA series from Sakamoto Yakuhin Kogyo Co. promote UV polymerization through acrylic functional groups and can be cured at room temperature with minimal energy and time, making them suitable for vat polymerization processes [22].

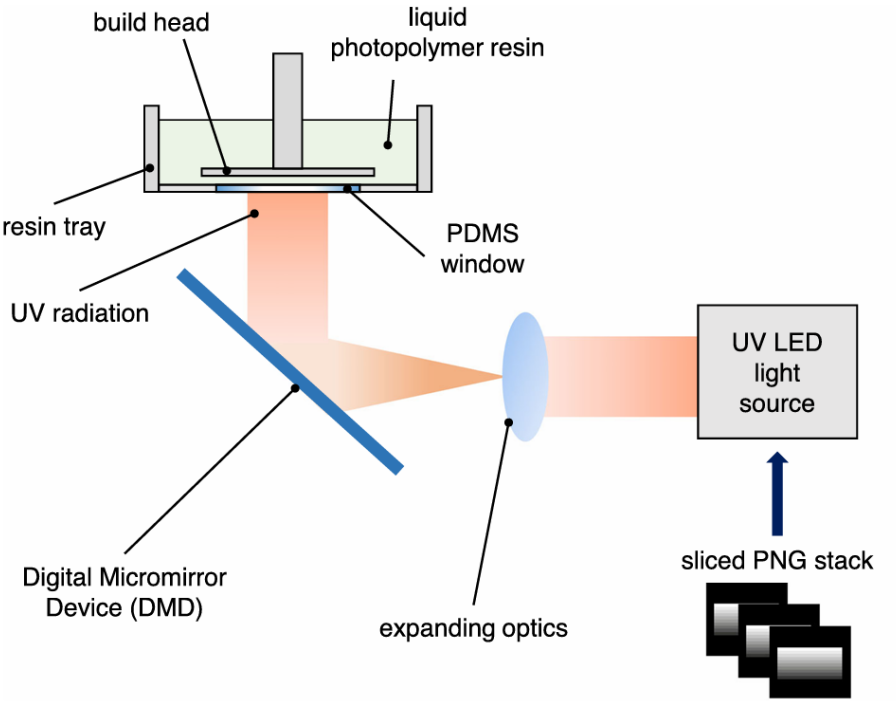

Figure 1.15 Schematic of DLP.

In addition, all these methods are carried out with post-processing, such as washing the printed part in a solvent bath with isopropyl alcohol, and further curing with UV light. These additional processes enable us to enhance mechanical properties of the final products. All methods need to consider some parameters, for example, speed, resolution and build volume.

The adverse relation between the feature size and the printing area for Vat Photopolymerization 3D printing technologies is displayed in Figure 1.13. More increasing the printing resolution, less printing area due to the price [23].

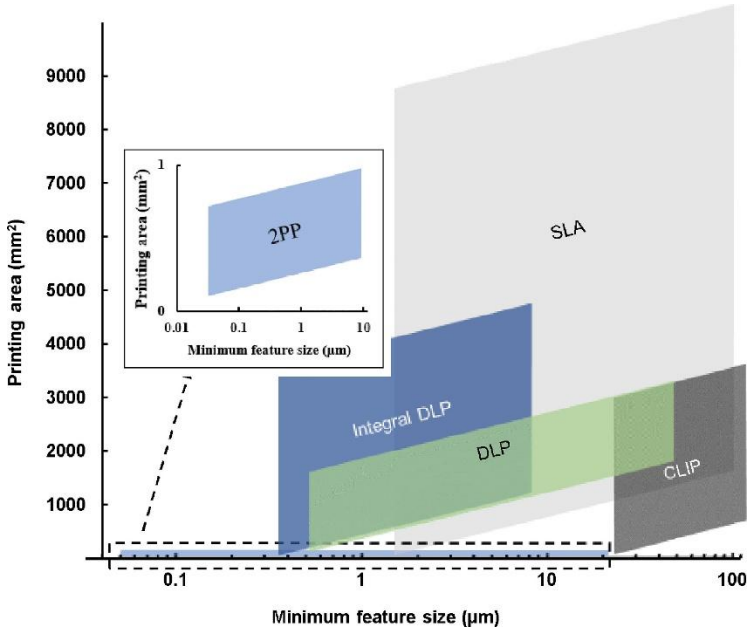

Figure 1.13 Plot showing the adverse relation between the feature size and the printing area for Vat Photopolymerization methods.

1.3 Overview of glycerol and photocurable materials

Glycerol represents one of the most useful bio-derived building blocks currently available for polymer science. Since they are owing to the presence of three hydroxyl (–OH) groups in its molecular structure, glycerol can participate in multiple chemical reactions, enabling its direct use as a multifunctional monomer or as a plasticizing component in a wide variety of polymer systems. This intrinsic trifunctionality makes glycerol particularly attractive for synthesizing highly crosslinked polymer networks with designable mechanical and thermal properties.

From a sustainability perspective, glycerol has gained even greater importance because it is generated in large quantities as a by-product during biodiesel production and purification. The reuse

of this surplus glycerol is not only economically advantageous, but also environmentally strategic, contributing to reducing waste and the development of circular material flows. Since they are non-toxic, biodegradable, and also highly biocompatible, glycerol-based polymers have been introduced for biomedical, environmental, and advanced manufacturing applications. Moreover, the use of glycerol as a renewable feedstock helps decrease dependence on fossil-derived resources, leading polymer production with global sustainability goals [24].

An effective strategy to enhance the functionality of glycerol-derived polymers is the acrylation of their hydroxyl groups. Through esterification reactions with acrylic or methacrylic derivatives, UV-responsive acrylate parts can be introduced into the polymer backbone. These acrylated glycerol-based systems become suitable for radical photopolymerization processes, which proceed rapidly under UV irradiation. UV curing is highly advantageous because it occurs at room temperature, requires relatively low energy input, and allows fast processing times compared to conventional thermal curing technologies.

An additional field of considerable interest is the production of acrylated polyglycerol monomers, which originate from naturally occurring triglycerides present in vegetable oils and animal fats. Triglycerides can be cleaved into glycerol and fatty acids through either saponification or hydrolysis. In the saponification route, triglycerides are treated with a strong alkaline solution, typically sodium hydroxide (NaOH) or potassium hydroxide (KOH), under heating conditions. This reaction yields glycerol along with the corresponding fatty acid salts, commonly referred to as soaps. Alternatively, hydrolysis can be performed under elevated temperature and pressure using water, and in some cases enzymatic catalysts such as lipases are employed to facilitate the reaction. This process produces glycerol and free fatty acids [25].

The glycerol obtained from these reactions can subsequently undergo polymerization via a condensation mechanism to form polyglycerol. During this step, glycerol molecules are heated in the presence of an appropriate catalyst, promoting dehydration reactions that lead to the formation of ether linkages between monomer units. By carefully adjusting reaction parameters such as temperature, catalyst concentration, and reaction time, it is possible to tailor the molecular weight of the resulting polyglycerol [25].

In the final stage, the hydroxyl groups of polyglycerol are functionalized through esterification with acrylic acid or its derivatives. This modification introduces acrylate functionalities onto the

polymer backbone, producing multifunctional UV-curable monomers. These materials can then be employed in a wide range of industrial, biomedical, and environmental applications.

Such characteristics make acrylated glycerol-based resins well suited for AM technologies, particularly Vat Photopolymerization techniques such as DLP and SLA. The rapid curing kinetics, combined with the possibility of fine structural control, enable the fabrication of complex 3D structures with high resolution and reduced material waste. Moreover, glycerol-based photocurable resins represent a promising class of sustainable materials capable of bridging green chemistry principles with advanced digital manufacturing technologies [26, 27].

1.4 Mechanism of thermochromism in PCDA-Based Polydiacetylene

Thermochromism materials are widely utilized in fields such as temperature indicators for food packaging and the management of medicines. Due to its potential of changing color at low temperatures, polydiacetylene (PDA) polymers have been studied and used in many sensing systems [28]

PDAs are obtained by 1,4-addition polymerization reaction of corresponding diacetylene monomers upon UV irradiation, resulting in alternating double and triple bonds. PDA is a conjugated polymer characterized by an extended π-electron system along its backbone. This extended π-conjugation enables delocalization of electrons, which is responsible for its optical color properties. [29]

PDA shows a blue color under normal conditions. The color will change to red in response for stimuli such as light, temperature, pH, pressure, solvent or interaction with biological agents [30-35]. At the normal condition with blue color, the polymer backbone adopts a highly planar conformation, which allows efficient π-electron delocalization along the conjugated chain. By elevating temperature, the polymer matrix structures move and change, leading to a distortion of the backbone conformation. At this moment of polymer, the effective conjugation length is reduced due to changes in intermolecular interactions and molecular packing. As results, the color of polymer changes from blue to red [36, 37].

10,12-pentacsadiynoic acid (PCDA) based thermochromic polymers among PDAs have studied a lot due to their fascinating reversible color transition as a function of temperature [38]. Various studies have reported reversible chromium at high temperatures [39-43].

This thermally induced conformational change is often triggered by variations in hydrogen bonding and side-chain mobility. Therefore, the thermochromic behavior of PCDA-based systems is closely related to both molecular structure and supramolecular organization. Some studies have been trying to conduct color transition at low temperature. For example, PCDA was attached to a phenolic-group and enabled to change the color irreversibly at low temperature [37]. However, there has been limited exploration of studies regarding low-temperature ranges and thermochromic properties.

1.5 Purpose and scope of this work

Previous studies have evaluated the reactivity and rheological properties of acrylated polyglycerol resins (SYntech SA series) and demonstrated their suitability as UV-curable materials for 3D printing, as well as the feasibility of fabricating electrically conductive composites by incorporating carbon nanotubes. On the other hand, polydiacetylene-based materials have been extensively studied as stimulus-responsive systems due to their distinct color change from blue to red upon UV-induced polymerization. However, most existing studies have focused on thermochromic behavior at relatively high temperatures, and the development of materials exhibiting color change in the low-temperature range has not been limited [37, 44].

In this study, considering the increasing demand for sustainable materials and environmentally friendly manufacturing methods, DLP-based 3D printing was performed using a UV-curable resin composed of biobased acrylate polyglycerol with PCDA. The effects of PCDA content on printability and thermochromic behavior of the printed objects were systematically investigated. This study aims to provide fundamental insights into the design of functional, bio-based photocurable materials and demonstrate their potential in advanced additive manufacturing applications.

2 Materials and Methods

2.1 Materials

SYntech SA Series SA-TE 60, a polyglycerol-based acrylate monomer, was used as the resin matrix, procured from SakamotoYakuhin Kogyo Co., Ltd. (Osaka, Japan)., with the molecular weight of 3000 g/mol [45]. Phenyl-bis(2,4,6-trimethylbenzoyl) phosphine oxide (BAPO) used for photoinitiator, and 10,12-pentacsadiynoic acid (PCDA) used for the thermochromic polymer, were purchased from Sigma-Aldrich (Milano, Italy). The general chemical structures of those materials are shown in Figure 2.1.

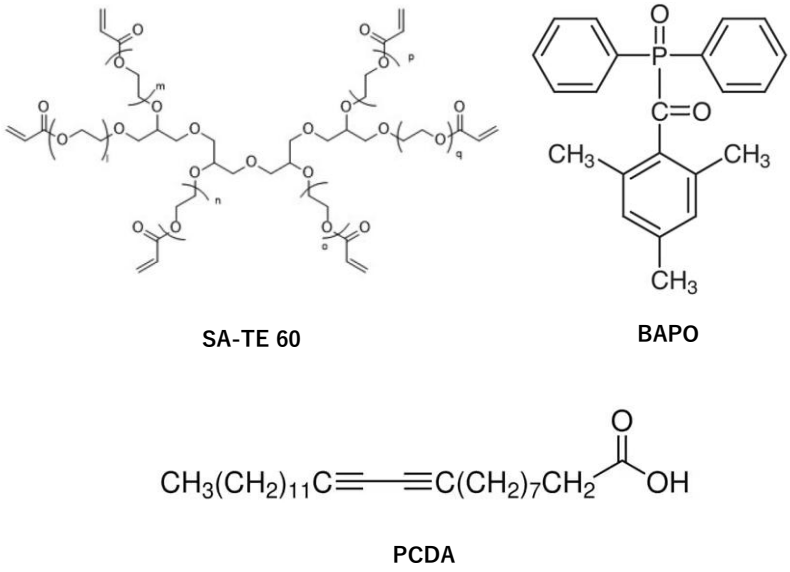

Figure 2.1 Chemical structures of materials

2.2 Formulation preparation

SA-TE 60 was mixed with 1 phr of BAPO in an ultrasonic bath at 40 °C until BAPO was dissolved completely. The formulation container was covered with aluminum paper to avoid light contact. Then, PCDA was mixed with the formulation in weight percentages of 0.25, 0.50, and 0.75 wt %, using a homogenizer ULTRA-TURRAX T10 basic (Savitec. Torino, Italy). The program selected is the following: 1 min mixing at 1000 rpm for 5 times, 1 min interval each mixing in order not to heat the formulation by vibration of the machine.

2.3 Characterizations

Characterization of both liquid formulations and printed samples were investigated. The following tests were carried out:

1. Fourier Transformed Infrared spectroscopy (FT-IR) conducted for the liquid formulations to confirm the conversion after UV irradiation at different exposure time.
2. Rheology tests for liquid formulations to find the relation between shear rate and viscosity and discover which samples are suitable for 3D printing.
3. Differential Scanning Calorimetry (DSC) and Dynamic Mechanical Thermal Analysis (DMTA) were conducted to measure the thermal properties, especially the behavior of glass transition.
4. With a bottom-up DLP 3D printer, three different structures were fabricated to ensure its printable potential.
5. The color transition from blue to red of printed structures was observed using the thermometer and recorded the videos.

2.3.1 FT-IR spectroscopy

Fourier Transform Infrared Spectroscopy (FT-IR) is an analysis that takes advantage of the interaction between infrared electromagnetic waves and the molecules within a sample. When infrared photons are absorbed, their energy is converted into vibrational energy of the molecules. Since each type of chemical bond possesses its own characteristic vibrational mode, the resulting IR absorption spectrum provides information related to the chemical structures of the material. The spectrum is presented with the wavenumber [cm^{-1}] on the horizontal axis and the absorbance [%] on the vertical axis.

FT-IR analysis was carried out to confirm the crosslinking process and assess the conversion of the resin after exposure to the UV light. The Thermo Scientific TM NicoletTM iS50 FTIR spectrometer and Omnic TMSpectra software were used to conduct the analysis, and Hamamatsu LC8 lamp was adopted for conducting photo-crosslinking. The formulations were spread on a SiC substrate using a spread bar to form films approximately 12 μm. The IR spectrum of each sample was first measured without exposing the UV light (pre-curing, t = 0 s). Then the films were irradiated with the

UV light for 1, 3, 5, 10, 30, 60, 90, 120 and 180 s at 5 cm distance and at 1 % intensity of lamp, corresponding to an irradiation energy of around 10 mW/cm^2. The IR spectrums were recorded after each irradiation interval with exposure time. The conversion percentage was subsequently tracked and plotted as a function of the UV exposure time from 0 to 180 s. The conversion was calculated using the below equation (1):

$$Conversion\ (\%) = \frac{\left(\frac{A_{fun}}{A_{ref}}\right)_{t=0} - \left(\frac{A_{fun}}{A_{ref}}\right)_t}{\left(\frac{A_{fun}}{A_{ref}}\right)_{t=0}} \times 100 \quad (1)$$

where A_{fun} is the area of the acrylate group at 810-820 cm^{-1}: the carbon-carbon double bond, while A_{ref} is the area of the reference group at 2800-3000 cm^{-1}: C-H stretching [37, 44, 46, 47].

2.3.2 Rheology

To observe the behavior of rheology and viscosity of formulations, rheological measurements were carried out by using Anton PAAR Modular Compact Rheometer (Physica MCR 302, Graz, Austria). The viscosity of the formulation should be clear to ensure which ones are more suitable for 3D printing processes. A 1 mm gap was set for the rheological measurements, and viscosity was recorded over a shear-rate range of 0.01-1000 s^{-1} at a constant frequency of 1 Hz at room temperature. Viscosity values were reported as a function of shear rare.

2.3.3 DSC

Differential Scanning Calorimetry (DSC) analysis was done with the Merler TOLEDO DSC-1 instrument. This test has been used to define the glass transition temperature (T_g) of each sample. The samples (approximately 10 mg) were sealed in Al pans and measured under N_2 atmosphere, and the flow rate was 40 mL/min. The temperature was scanned from -60 to 100 °C at a heating rate of

3 °C/min. After erasing the previous thermal history during the first heating, T_g was determined from the onset of the heat capacity change in the second heating curve.

2.3.4 DMTA

Dynamic Mechanical Thermal Analysis (DMTA) was conducted by using a Triton Technology instrument in the tension mode under a uniaxial stress at a frequency of 1 Hz. Liquid nitrogen was used to cool the chamber to the initial test temperature, which was approximately -60 °C. The samples used for DMTA were rectangular specimens prepared by mold casting.

DMTA enables the evaluation of the viscoelastic behavior of polymeric materials. The resulting deformation consists of an elastic component; represented by the storage modules E', and a viscous component; represented by the loss modules E" when a cyclic stress is applied. The ratio between these two quantities defines the damping factor (tan δ). Among the curves obtained from the analysis, the temperature dependence of tan δ is directly provided by instrument software. T_g of each sample was identified as the temperature corresponding to the peak of the tan δ curve.

2.4 3D-printing via DLP technology

The printability ware evaluated using a Prusa SL1S 3D printer with a 405 nm UV light source. It is a DLP-type printer with a digital mask, exploiting a light source emitter. The layer thickness was fixed at 0.05 μm, and the exposure time reported in Table 3.2. The irradiation time varied for each formulation, considering the content of PCDA for proper spread of the permutations and accurate construction.

Especially, the exposure time of the first layer should be separated from that of the other layers. It is mostly because the first layer must allow adhesion between two interfaces: the metal platform surface and the composite structure being built by the printer. Thus, the first layer was exposed to the light longer than other layers. In addition, the needed exposure time increased by the increasing of viscosity and the UV absorption with higher content of PCDA (filler).

The printed samples are for DMTA and DSC analysis. Specimens for DMTA were 18×8×1 mm^3, and approximately 10 mg of printed sample were cut from them for the DSC analysis. To demonstrate the printability of the formulations, some complex geometries built such as star shape, chunk gyroid and twisted cage which surrounded with diagrid side surface. After obtaining the samples, they were cleaned by ethanol or isopropanol to remove unreacted residual monomers.

The printed structures then heated to assess the color transition from blue to red with the thermometer. The color changes were recorded as video. Samples were set on the heater at room temperature, and the temperature was elevated until the color transition of samples completely had done.

3 Results and discussions

In this section, the results and consideration of both liquid formulations and 3D-printed samples were reported.

3.1 FT-IR spectroscopy

SA-TE 60–BAPO formulations containing 0, 2.5, and 5.0 wt% PCDA were subjected to infrared spectroscopy (FT-IR) and measurements were performed after UV irradiation at various exposure times (0, 1, 3, 5, 10, 30, 60, 120, and 180 s). The obtained FT-IR spectra for all samples are shown in Figure 3.1, 3.2 and 3.3. As shown in those figures, all spectrums have exhibited similar trends.

The peak at the carbon-carbon double bond at 810–820 cm^{-1}, corresponding to the characteristic of the acrylate group, decreased markedly with increasing UV-induced crosslinking. The peak was chosen as the functional one due to its significant change during the cross-linking processes.

In contrast, the peak at 2800–3000 cm^{-1}, assigned to C–H stretching, remained nearly unchanged during the crosslinking reaction and was therefore used as a reference.

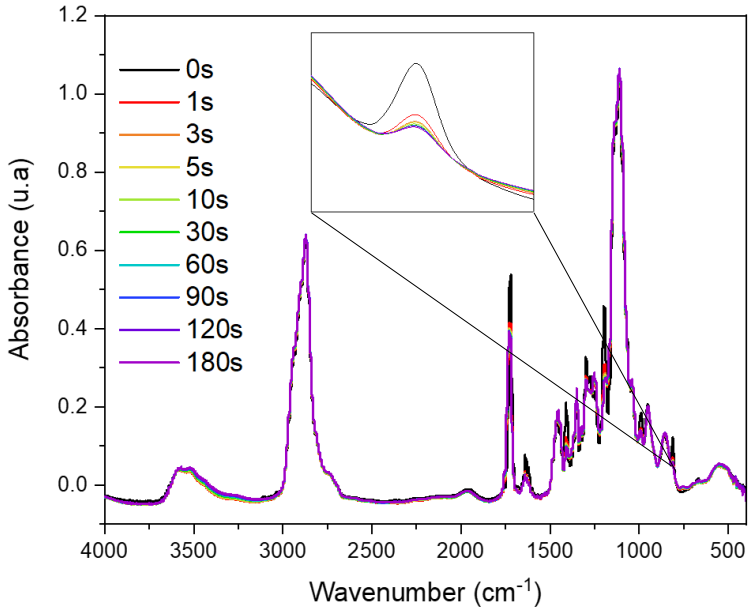

Figure 3.1 FT-IR spectrum of SA-TE 60-BAPO.

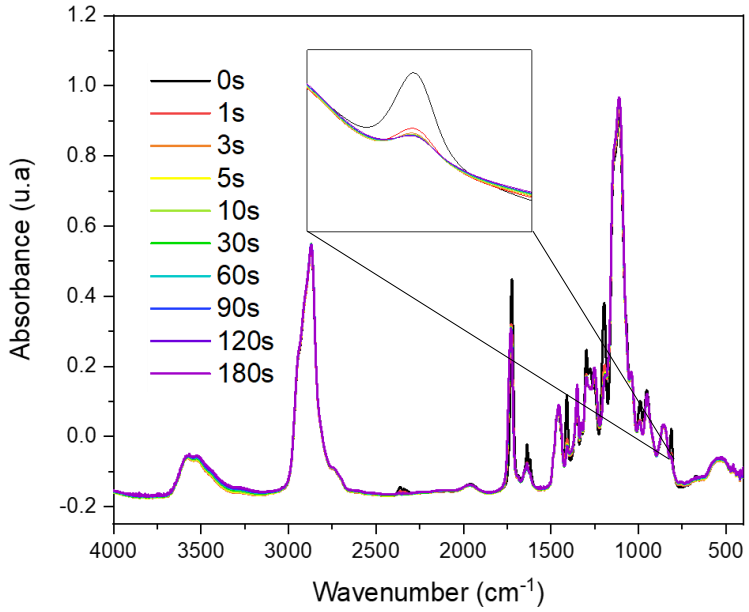

Figure 3.2 FT-IR spectrum of SA-TE 60-BAPO with 2.5 wt% PCD

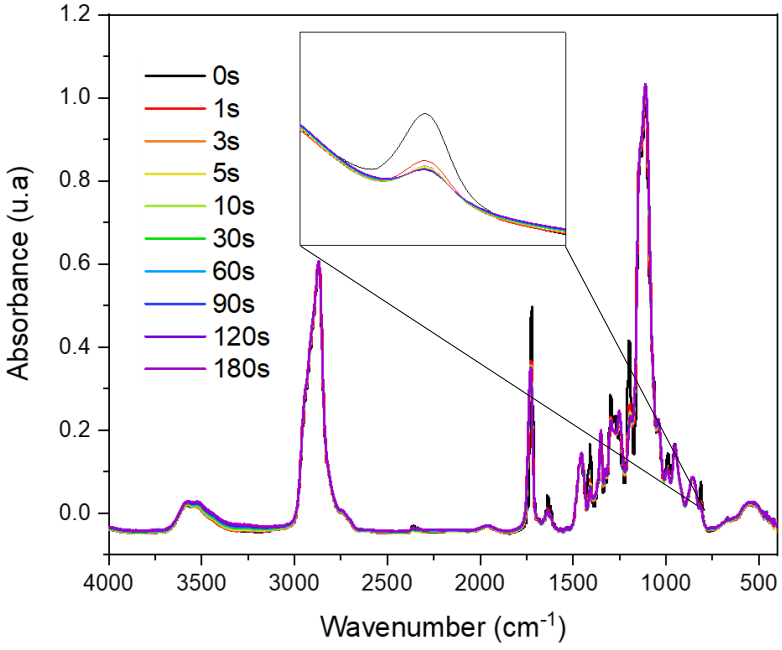

Figure 3.3 FT-IR spectrum of SA-TE 60-BAPO with 5.0 wt% PCDA.

Using equation (1) shown in Section 2.3.1, the conversion was calculated by taking the area of the characteristic peak of the C=C bond as A_{fun} and that of the C–H bond as A_{ref}. This calculation was performed for all formulations. Figure 3.4 shows the conversion curves as a function of irradiation time for each formulation, and Table 3.1 summarizes the conversion values after 180 s of UV exposure.

As these results indicate, the conversion decreased as the PCDA content, the filler in the photocurable formulation increased. This was attributed to the absorption of UV light by PCDA, which reduces the amount of UV light available for the photoinitiator, as well as to the increased viscosity caused by higher PCDA loading, which restricted the mobility of carbon chains and hindered their reaction with the photoinitiator and affecting the photopolymerization process.

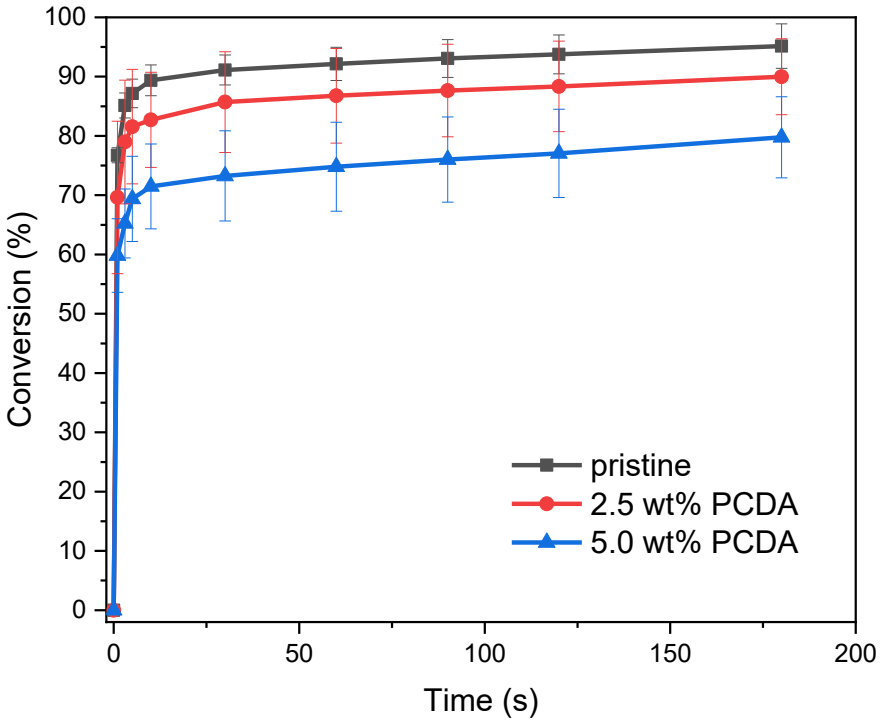

Figure 3.4 Conversion grade of SA-TE 60-BAPO with different PCDA content

Table 3.1 Conversion grade after 180 s of UV irradiation for all the studied formulations

Formulation	**Conversion at 180 s [%]**
0 wt% PCDA	95
2.5 wt% PCDA	90
5.0 wt% PCDA	80

3.2 Rheology

Rheological measurements were conducted to evaluate the viscosity and dynamic behavior of the formulations and to identify compositions suitable for bottom-up DLP 3D printing. Figure 3.5 shows the viscosity curves of formulations with different PCDA contents as a function of the applied shear rate.

The yellow region in Figure 3.5 indicates the viscosity range suitable for DLP 3D printing (0.2–10 Pa·s) and the typical shear-rate range occurring during the printing process (5–20 s^{-1}). As shown in Figure 3.3, the formulations with 0, 2.5 and 5.0 wt% PCDA examined were confirmed to be sufficiently printable. In fact, within the specified shear-rate range, the viscosities of formulations with 0, 2.5 and 5.0 wt% PCDA fall within the yellow region, which serves as an indicator of printability. For the formulation with 7.0 wt% PCDA, it showed higher viscosity than others and the viscosity at low shear rate range was out of the yellow area in Figure 3.5.

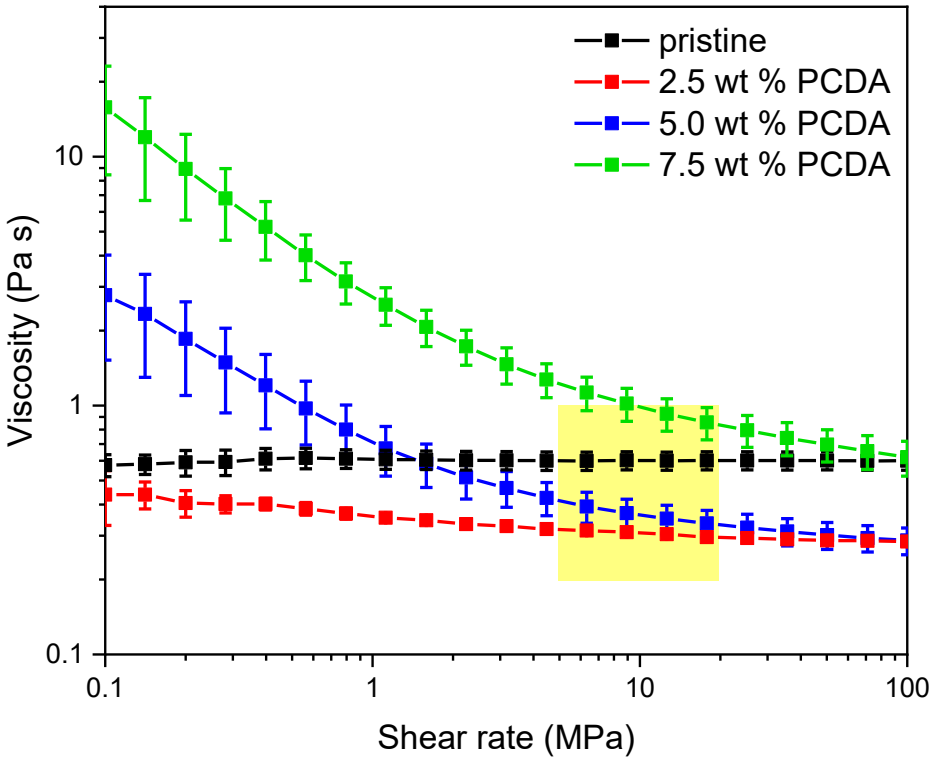

Figure 3.5 Viscosity curves as a function of the shear rate of SA-TE 60-BAPO varying PCDA content.

As the PCDA content increased, a shear-thinning behavior, where the viscosity decreases with increasing shear rate, became clearly. Shear-thinning refers to the rheological behavior in which the polymeric networks and intermolecular interactions formed within the fluid are disrupted upon the application of shear, thereby promoting flow and reducing viscosity. With higher PCDA content, stronger interactions within polymeric network led to higher viscosity in the low-shear rate area, whereas these structures are more readily broken under high shear, resulting in a huge decrease in viscosity.

As shown in Figure 3.5, the shear-thinning behavior appeared for the formulations with 5.0 and 7.5 wt% PCDA. Due to this phenomenon, the former could be able to decrease its viscosity, considered as suitable for printing; while the latter possessed relatively high viscosity even though it exhibited large decreased viscosity.

3.3 DSC

From this section, the topic changes from liquid formulations to solid samples.

DSC analysis was conducted for each formulation and PCDA powder to assess the thermodynamic properties, especially finding out T_g of each sample and PCDA. The heat curves of formulations with different PCDA content are shown in Figure 3.6, and the DSC curve of PCDA powder is shown in Figure 3.7.

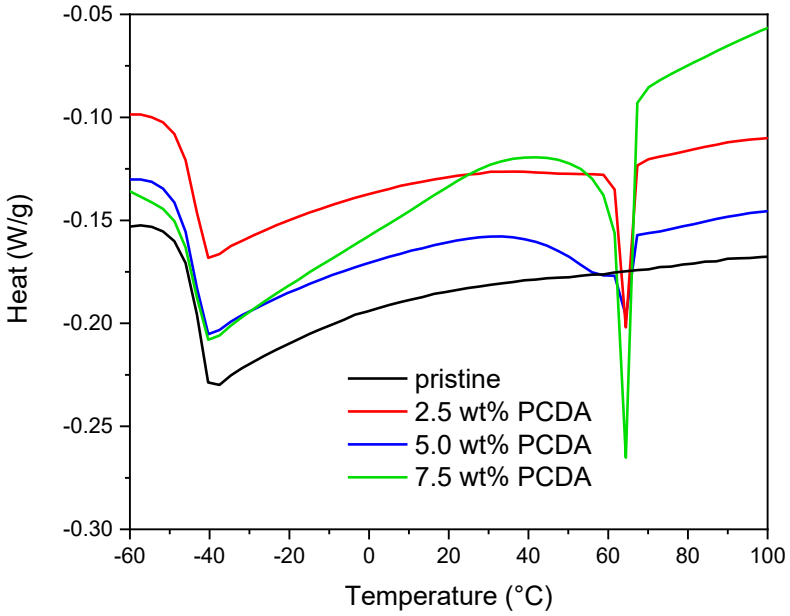

Figure 3.6 DCS plots of SA-TE 60-BAPO with different PCDA content

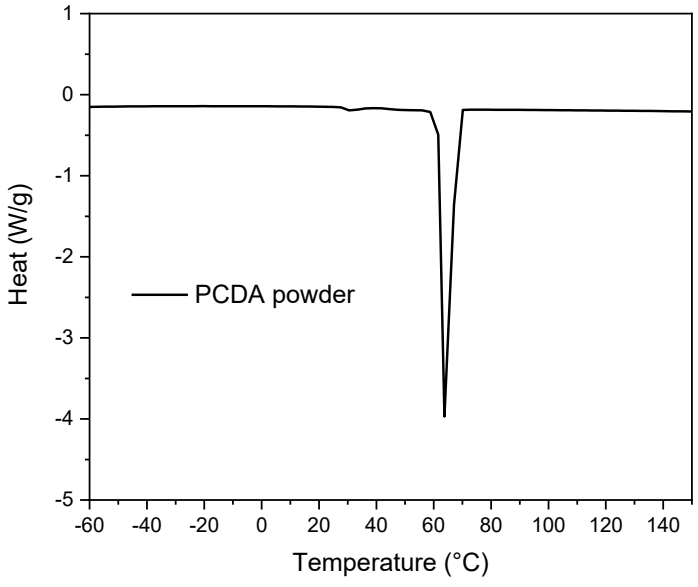

Figure 3.7 DSC plot of PCDA powder

As shown in Figure 3.6, two thermal transitions were observed: one at the lower temperature region (around −40 °C) and another at the higher temperature region (around 60 °C). The low-temperature transition is attributed to the glass transition of the flexible aliphatic segments in the acrylated resin, whereas the high-temperature transition corresponds to the glass transition of the cross-linked polymer network. These transitions originated from the polymer matrix and although the addition of PCDA influenced position or shape of these transitions, no distinct thermal transition attributable to PCDA itself was observed in the cured samples.

In contrast, the DSC curve of PCDA powder shown in Figure 3.7 exhibits a distinct thermal peak originating from the intrinsic thermal behavior of crystalline PCDA, such as a solid–solid phase transition or a melting-related transition. This thermal behavior is clearly different from that of the cured polymer systems shown in Figure 3.6. These results suggest that PCDA does not form a continuous crystalline phase in the cured materials but is dispersed within the matrix.

3.4 DMTA

DMTA analysis was carried out for each formulation. Figure 3.8 shows the curves of tan (δ) and Storage Modules E' as a function of temperature for all the formulations studied.

Figure 3.8 shows the temperature dependence of the storage modulus (E′) and tan δ for SA-TE 60–BAPO formulations containing different amounts of PCDA. The results indicate that neither E′ nor tan δ changes monotonically with increasing PCDA content, and no simple proportional relationship is observed. This behavior arises from the simultaneous action of multiple effects introduced by PCDA.

Dispersed PCDA within the matrix can partially restrict the segmental motion of the polymer chains, leading to localized increases in stiffness and modifications of the glass transition behavior. However, PCDA aggregation or domain formation at higher loadings can reduce stress transfer efficiency and generate structural heterogeneities, resulting in deviations from the behavior expected for a simple reinforcing filler.

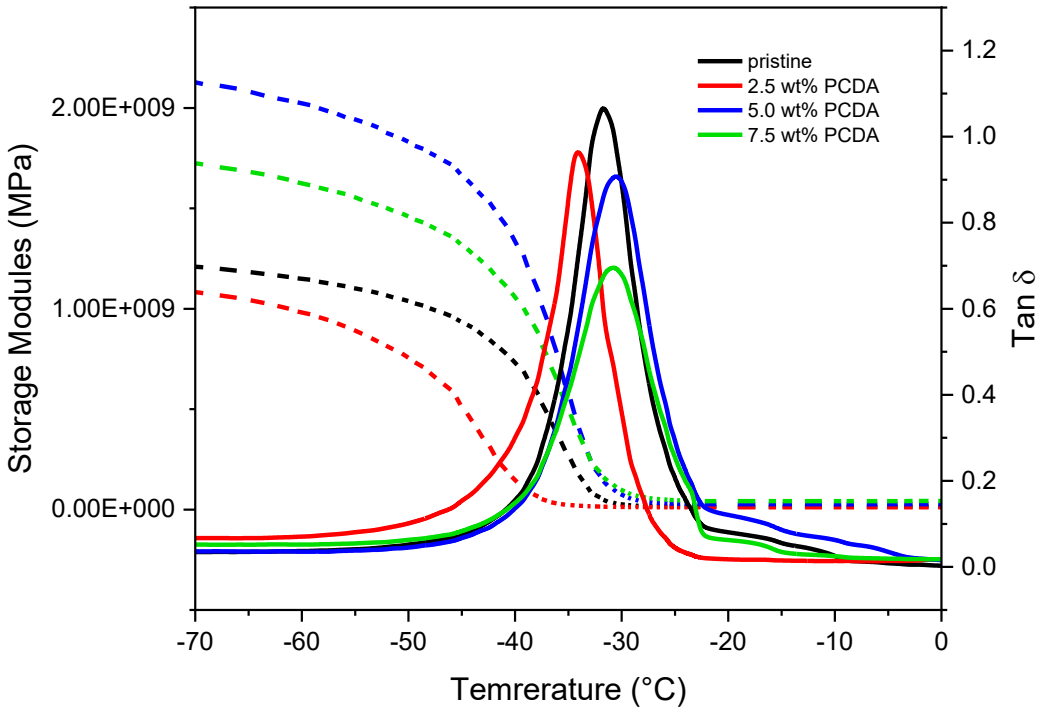

Figure 3.8 Tanδ and Storage Modules curves as a function of temperature for SA-TE 60-BAPO with different PCDA content.

A similar competition is observed in the tan δ response. Interfacial interactions between PCDA and the matrix suppress molecular mobility and decrease damping, whereas a reduction in effective crosslink density and the presence of PCDA rich regions broaden the relaxation time distribution and increase damping. Consequently, the maximum tan δ and the peak shape do not show a straightforward correlation with PCDA content.

Overall, these results suggest that PCDA does not behave solely as a rigid filler, but instead influences the viscoelastic response through a combination of localized reinforcement, aggregation induced heterogeneity, and modifications to the crosslinked network structure.

3.5 3D-printing structures via DLP technology

During the printing processes, the printing parameters shown in Table3.2 were used, depending on the amount of PCDA filler in the formulation. Since PCDA powder is light material, the amount of it in the formulation with 7.0 wt% of PCDA is almost dominant component though it is a filler. Moreover, as already mentioned in section 3.2, the viscosity of the formulation was higher than it required for proper printing. Thereby the formulation with 7.0 wt% of PCDA was considered unsuitable for printing.

With increasing PCDA content, all the parameters listed in Table 3.2 had to be increased to achieve successful printing. This requirement arises from the higher viscosity of the formulations and the enhanced UV-absorption effect associated with higher PCDA loadings. Using the formulations identified as printable through rheological analysis, sample fabrications were carried out by DLP printing. The printed structures are shown in Figure 3.9

Table 3.2 Printing parameters adopted as a function of the formulation type.

Samples	Bottom exposure time (s)	Exposure time for each layer (s)
2.5 wt% PCDA	5	2
5.0 wt% PCDA	8	5

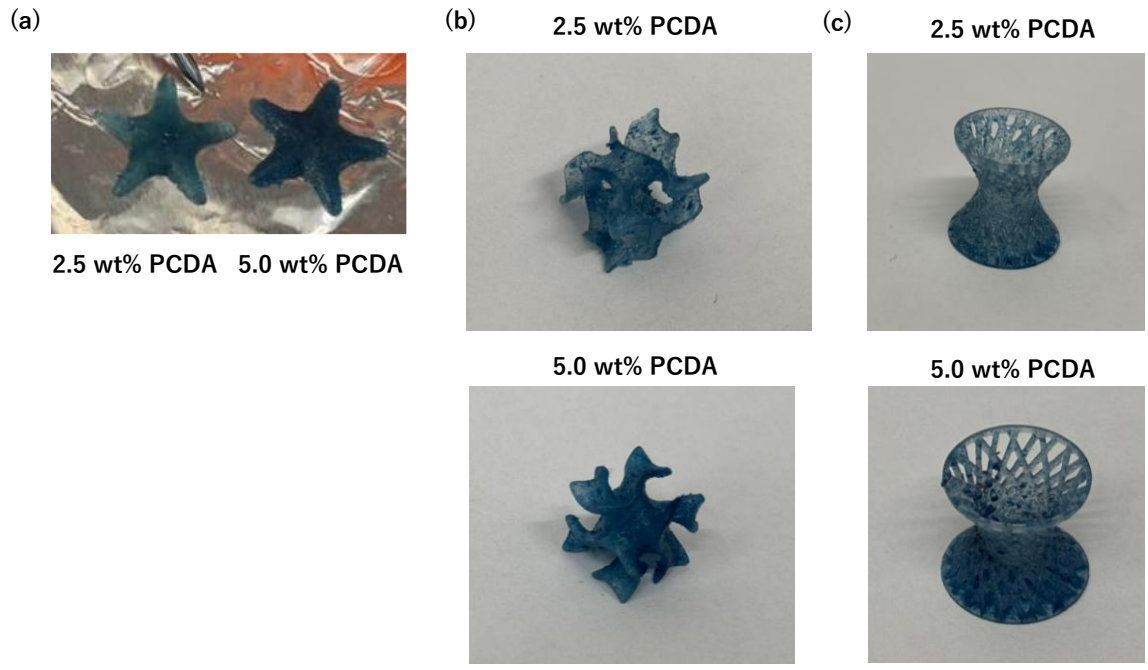

Figure 3.9 3D printed structures by DLP printing: (a) star shape, (b) chunk gyroid and (c)twisted cage.

The thermochromism analysis of 3D printed structures by elevated temperature are shown Figure 3.10. The color changes by heating have been observed with star shape samples. These samples exhibited a clear thermochromic response arising from temperature-induced distortions in the polymer main chain. In the blue phase, the conjugated backbone maintains a high degree of planarity. However, upon heating, the backbone undergoes twisting, leading to a reduction in conjugation length and a corresponding blue shift in the absorption band, ultimately resulting in a transition from blue to the red phase.

As shown in Figure 3.10, heating above 25 °C induced a phase transition of PCDA into its thermally treated form, accompanied by a color change from deep blue to red. This behavior is attributed to thermally driven structural relaxation of the main chain and the consequent disruption of π-conjugation.

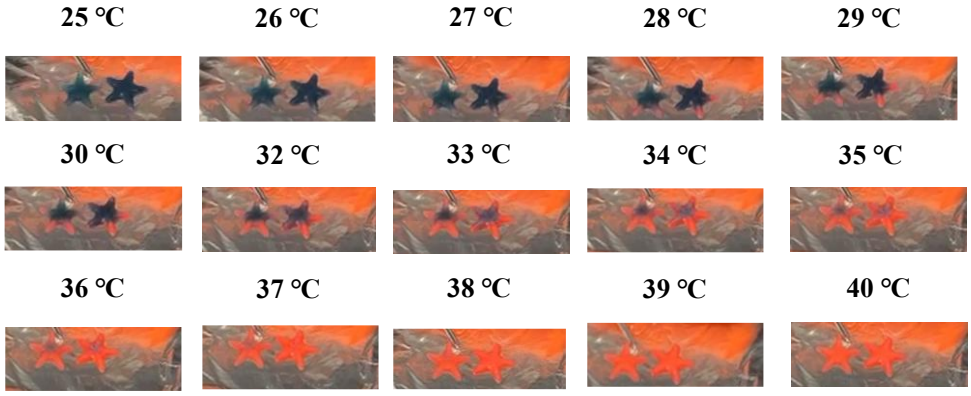

Figure 3.10 Thermochromism analysis of 3D printed structures with different PCDA content.

4 Conclusions

In this study, 3D-printed structures were fabricated using a UV-curable resin composed of bio-based acrylated polyglycerol monomer (SA-TE 60) containing PCDA, and their thermochromic behavior was systematically investigated. FT-IR analysis revealed that increasing the PCDA content led to a decrease in acrylate conversion due to enhanced UV absorption by PCDA and the viscosity increase that restricted chain mobility during photopolymerization. Rheological measurements confirmed that all formulations fell within the viscosity range suitable for DLP printing, while higher PCDA loadings exhibited pronounced shear-thinning behavior.

DSC and DMTA analyses indicated that PCDA does not form a continuous crystalline phase within the cured network but is instead dispersed throughout the matrix. The addition of PCDA influenced the glass transition behavior and viscoelastic response through a combination of localized restriction of chain mobility, aggregation-induced heterogeneity, and modifications to the crosslinked network structure, rather than acting as a simple rigid filler.

During DLP printing, higher PCDA contents required increased exposure parameters due to elevated viscosity and stronger UV absorption. Nevertheless, formulations containing 2.5 wt% and 5.0 wt% PCDA were successfully printed. Thermochromic evaluation of the printed structures demonstrated a clear color change from deep blue to red upon heating above 25 °C, corresponding to the thermally induced phase transition of PCDA. This behavior was attributed to thermally driven structural relaxation of the conjugated backbone and the consequent disruption of π-conjugation.

Therefore, the results demonstrate that bio-based acrylate resins containing PCDA are compatible with DLP 3D printing and can impart thermochromic functionality capable of recording thermal history. This study highlights the potential of such materials for applications in temperature-sensitive packaging and safety-monitoring devices, contributing to the development of functional 3D-printed materials that integrate bio-based polymers with stimulus-responsive systems.

References

[1] S. Luo, Q. Zhang, L. Zhu, H. Lin, B. A. Kazanowska, C. M. Doherty, A. J. Hill, P. Gao, R. Guo, *Chem. Master.*, **30**, 5322-5332 (2018).

[2] J. G. Rosenboom, R. Langer, G. Traverso, *Nat. Rev. Mater.*, **7**, 117-137 (2022).

[3] A. B. Unni, T. M. Joseph, *Polymers*, **16**, 1769 (2024).

[4] N. Shahrubudin, T. C. Lee, R. Ramlan, *Procedia Manuf.*, **35**, 1286-1296 (2019).

[5] M. Jiménez, L. Romero, I. A. Domínguez, M. d. M. Espinosa, M. Domínguez, *Complexity*, **1**, 9656938 (2019)

[6] J. Oh, *Maxillofac. Plast. Reconstr. Surg.*, **40**(1):2, (2018).

[7] P. K. Gokuldoss, S. Kolla, J. Eckert, *Materials*, **10**, 672 (2017).

[8] P. H. Salame, N. Ananya, H.S. Haran, S. R. Pillai, B. Kulsange, *Addit. Manuf. and Technol.***23***,* 563-597 (2024).

[9] L. A. A. Calderón, B. Graf, B. Rehmer, T. Petrat, B. Skrotzki, M. Rethmeier, *Adv. Eng. Mater.*, **24**(6), (2024).

[10] N. Chen, C. He, S. Pang, *J. Mater. Sci. Technol.*,**127**, 29-47 (2022).

[11] 3D Hubs. How to Design Parts for Material Jetting 3D Printing. 3D Hubs. Available online: https://www.3dhubs.com/knowledge-base/how-design-parts-material-jetting-3d-printing (accessed on [insert access date]).

[12] S. Parchegani, H. Piili, A. Ganvir, A. Salminen, *IOP Conf. Ser. Mater. Sci. Eng.*, **1296**(1), (2023).

[13] P. Dudek, A. Rapacz-Kmita, *Arch. Metall. Mater*., **61**(2), (2016).

[14] V. Pateloup, P. Michaud, T. Chartier, *Open Ceram*, **6**, 100132 (2021).

[15] F. Zhang, L. Zhu, Z. Li, S. Wang, J. Shi, W. Tang, N. Li, J. Yang, *Addit. Manuf.*, **48**, 102423 (2021).

[16] S. Zakeri, M. Vippola, E. Levänen, *Addit. Manuf.*, **35**, 101177 (2020)

[17] A. R. Johnson, C. L. Caudill, J. R. Tumbleston, C. Bloomquist, K.A. Moga, A. Ermoshkin, et al, *PLoS ONE*, **11**(9): e0162518 (2016).

[18] Z. F. Rad, P. D. Prewett, G. J. Davies, *Microsysyt. Nanoeng.*, **7**(71), (2021).

[19] R. V. Pazhamannil, P. Govindan, *Mater. Today Proc.*, **43**(1), 130-136 (2021).

[20] K. Sekmen, T. Rehhein, M. Johlitz, A. Lion, A. Constantinescu, *Continuum Mech. Thermodyn.*, **36**, 351-368 (2024).

[21] D. Chekkaramkodi, L. Jacob, M. C. Shebeeb, R. Umer, H. Butt, *Addit. Manuf.*, **86**, 104189 (2024).

[22] N. Ballard, J. M. Asua, *Prog. Polym. Sci.*, **79**, 40-60 (2018).

[23] A. Amini, R. M. Guijt, T. Themelis, J. De vos, S. Eeltink, *J. Chromatogr.* A, **1692**, 463842 (2023).

[24] N. B. Chamer, C. N. Bowman, Materials and Nanoscience Subject Collection; RSC Publishing, pp. 1-27 (2013).

[25] B. Hanganu, A. A. Velnic, V. P. Ciudin, D. Crauciuc, C. L. Buhas, I. S. Manoilescu, L. G. Solovastru, B. G. Ioan, *Rev. Chim.*, **68**(12), 2948-2951 (2017).

[26] S. Goyal, N. B. Hernández, E. W. Cochran, Polym. Int., 70(7), 911-917 (2021).

[27] A. R. You, J. Y. Kim, S. W. Ryu, ChemistrySelect 2023.

[28] X. Qian, B. Städler, *Chem. Mater.*, **32**, 1196-1222 (2019).

[29] H. Ko, D. G. Kang, Y. J. Choi, Y. Wi, S. Kim, H. H. Pham, K. M. Lee, N. P. Godman, M. E. McConney, K. U. Jeong, *J. Am. Chem. Soc.*, **146**, 4393-4401 (2024).

[30] G.Xi, L. Sheng, S. X. A. Zhang, *Mater. Sci. Eng.*: R: Reports **158**, 100774 (2024).

[31] S. Goyal, D. Sharma, A. Deep, K. Kumar, A. L. Sharma, *ACS Appl. Polymer Mater.*, **6**, 4186-4194 (2024).

[32] T. Pattanatornchai, J. Rueangsuwan, N Phonchai, N. Traiphol, R. Traiphol, *Colloids. Surf.*, A **594**, 124649 (2020).

[33] B. Das, S. Jo, J. Zheng, J. Chen, K. Sugihara, *Nanoscale*, **14**, 1670-1678 (2022).

[34] D. E. Wang, C. Yan, S. Bai, Y. Zhang, W. Huo, K. Ning, L. Zhao, H. Yang, H. Xu, *Chem. Eng. J.*, **483**, 149215 (2024).

[35] W. Chen, S. Hazoor, R. Madigan, A. A. Adones, U. K. Chintapula, K. T. Nguyen, L. Tang, F. W. Foss, H. Dong, *Mater. Today Adv.*, **16**, 100288 (2022).

[36] N. Ahmadi, D. Y. Kim, S. S. Shin, S. Daradmare, J. M. Kim, B. J. Park, *Small Structures,* **6**, 2400340 (2024).

[37] S. Goyal, D. Sharma, A. L. Sharma, K. Kumar, *Chemical Physics Impact*, **10**, 100803 (2025).

[38] O. Mapazi, P. K. Matabola, R. M. Moutloali, C. J. Ngila, *Sens. Actuators* B, **252**, 671-679 (2017).

[39] T. Liu, Z. Liu, Z. Fang, J. Zhang, S. Gong, J. Li, *Compos. Part B: Eng.*, **224**, 109191 (2021).

[40] Z. Ge, Z. Pan, S. Yan, B. Zhang, X. Shen, M. Wang, X. Ge, *Chin. Chem. Lett.*, **35**, 109850 (2024).

[41] X. He, F. Xu, F. F. Chen, Y. J. Zhu, Y. Yu, ACS Appl, *Nano Mater.* **6**, 23390-23400 (2023).

[42] Y. Gao, Z. Zhao, X. Huang, H. Xing, G. Yang, *Macromol. Res.*, **32**, 253-259 (2024).

[43] X. Huang, J. Ji, G. Li, G. Yang, J. Hou, ACS Appl. *Polymer Mater.*, **4**, 6047-6053 (2022).

[44] M. Porcarello, S. Bonardd, G. Kortaberria, Y. Miyaji, K. Matsukawa, M. Sangermano, *ACS Appl. Polym. Mater.*, **6**(5), 2868-2876 (2024).

[45] K. Matsukawa, Y. Miyaji, S. Kawabata, M. Innovation Lab, Kyoto Institute of Technology, Kyoto, Japan, Sakamoto Yakuhin Kogyo, Co., Ltd., Osaka, Japan.

[46] R. V. Ghorpada, S. M. Bhosle, S. Ponrathnam,C. R. Rajan, N. N. Chavan, R. Harikrishana, *J. Polym.*

Res., **19**, 9811 (2012).

[47] G. Kuang, H. Bakhshi, W. Meyer, *J. Polym. Res.,* **30**, 141 (2023).

Acknowledgements

Most of all, I would like to express my deepest appreciation to Professor Marco Sangermano, the supervisor of the Double Degree Program between Kyoto Institute of Technology and Politecnico d Torino, and at the same time, the head of the lab in Italy. He always took care of me a lot and made efforts to ensure that I did not feel lonely. Thanks to his heartful support of both academic and emotional sides, I was able to work in the laboratory in a comfortable and supportive environment.

I am also deeply grateful to the members of his laboratory. I would like to thank Matilde and Alberto, who worked together with me in the lab. Even though they were busy with their own work, they supported me whenever I needed help.

I would like to express my sincere gratitude to Mr. Asaoka and Mr. Suzuki, who supported and advised me for two years in the laboratory at Kyoto Institute of Technology. They taught me not only how to conduct research in the laboratory, but also how to be a researcher. Without their guidance, I would not have been able to find my way to complete this thesis.

I would also like to thank Mr. Sakai, the supervisor of the Double Degree Program between KIT and Polito, who devoted great effort to supporting me and making my stay in Italy comfortable.

Furthermore, I am grateful to all the members of the laboratory at Kyoto Institute of Technology and to everyone who have been supporting me during my stay in Italy.

Finally, I would like to express my sincere gratitude to my family for supporting me. Especially, I am deeply grateful to my mother, who raised me and my sister all by herself. I truly appreciate everything she has done for me, including allowing me to live my student life without personal hardship and encouraging me to study in Italy.